Shock Waves (2014) 24:583–592
DOI 10.1007/s00193-014-0530-7

ORIGINAL ARTICLE

Visualization of the structure of an incident shock wave/turbulent boundary layer interaction

L. He · S. Yi · Z. Chen · Y. Zhu

Received: 3 April 2012 / Revised: 26 November 2012 / Accepted: 8 September 2014 / Published online: 14 October 2014

Abstract An experimental study of shock wave/turbulent boundary layer interaction at Mach 3 is performed. A newly-developed nano-tracer planar laser scattering technique is used to reveal three-dimensional instantaneous structures of the flow. Large-scale structures within the incoming turbulent boundary layer and the unsteady motion of the separation bubble and the reflected shock are visualized in the streamwise wall-normal plane. The temporal evolution of the flow structures as well as the interaction between the large-scale structures and the reflected shock are analyzed using two successive images. Instantaneous structures in streamwise-spanwise planes at different heights are also presented, thus revealing highly three-dimensional nature of the interaction.

Keywords Shock wave/turbulent boundary layer interaction · Coherent structures · Flow visualization · Unsteadiness

1 Introduction

The interaction between a shock wave and a turbulent boundary layer (SWTBLI) is of frequent occurrence in supersonic and hypersonic flows, which are of both fundamental and practical importance. With an increasing interest in supersonic and hypersonic vehicles, SWTBLI has become important in a number of external and internal aeronautical applications relevant to aircrafts, missiles, rockets and projectiles [1]. According to Smits and Dussauge [2], SWTBLIs can be classified into two types: compression corner interactions and incident shock interactions. The former case has been extensively studied for a wide variety of flow conditions and configurations. More recent reviews of this type of interaction can be found in Refs. [1,2]. The latter case, on the contrary, is less documented. However, both types of interaction show similar behavior, such as the low-frequency motion of the reflected shock wave when boundary layer separation is involved [3].

The preponderance of large-scale structures within the incoming turbulent boundary layer has been motivating researchers to investigate the relationship between these structures and the large-scale unsteadiness of SWTBLI. Therefore, experimentalists were always interested to visualize the structures of SWTBLI, which would help to better understand the underlying physical mechanisms of its unsteadiness. The schlieren, as well as shadowgraphy, technique is a relatively simple, widely used method of flow visualization. Chapman et al. [4] used high-speed schlieren and shadow photography to study the shock-induced turbulent separation, and noted that "turbulent separations were relatively steady". However, their remark is probably incorrect. Verma [5,6] used a laser schlieren system to detect the unsteady shock motion in a hypersonic SWTBLI. Debiéve et al. [7] also used schlieren imaging to investigate the perturbations of a bow shock in front of a spherical body due to an upstream-directed jet emanating from the stagnation point of the sphere. Because the spanwise averaging of density gradients takes place when using the schlieren and shadowgraphy techniques, the usefulness of these methods is relatively limited in case of axisymmetric or three-dimensional flowfields. Nevertheless, these methods are still used together with other measurement methods in experimental studies [8–10].

Communicated by H. Olivier and E. Timofeev.

L. He (✉) · S. Yi · Z. Chen · Y. Zhu
College of Aerospace and Material Engineering, National University of Defense Technology, Changsha 410073, China
e-mail: helin.101sys@gmail.com; helin@nudt.edu.cn

With the recent advances in laser diagnostic techniques, the planar laser scattering (PLS) technique has become a popular tool for flow visualization. This technique, which avoids the spanwise integration effects of schlieren photography and shadowgraphy, is typically used to image large-scale turbulent structures in shear layers and boundary layers [11–16]. Besides, this technique provides higher spatial resolution to measure shock positions than the wall pressure measurements. It is possible to study the relationship between shock fluctuations and large-scale structures within the upstream boundary layer. Chan [17] and Beresh et al. [18] used the instantaneous planar laser scattering from condensed alcohol fog to examine the relationship between the incoming boundary layer thickness and the large-scale shock motion, and found no significant correlation between them. Ganapathisubramani et al. [19] also used the acetone PLS to study the effect of the upstream boundary layer on the unsteadiness of shock-induced separation. A megahertz rate visualization system based on PLS was used to study a corner interaction at Mach 2.5 by Wu and Miles [20]. The authors reported that "the shock motion is strongly correlated with the incoming boundary layer structure". However, many previous studies (see, e.g., [1,21,22]) reported that the time scale of the shock motion is of the order of 10 $\delta/U_\infty - 100\,\delta/U_\infty$ (where δ is the incoming boundary-layer thickness and U_∞ is the free-stream velocity), in contrast to the characteristic time scale of the incoming boundary layer, δ/U_∞. The cause of the low-frequency unsteadiness is still an open question, in particular, whether or not the low-frequency shock motion is associated with large-scale structures within the upstream boundary layer. Therefore, more experiments are needed to provide detailed information on the nature of SWTBLIs.

A newly developed technique, called nano-tracer planar laser scattering (NPLS), was recently used to visualize large-scale turbulence structures within high-speed flows, such as mixing layers [23,24] and boundary layers [25]. A detailed description of this technique is provided in the next section. The aim of the present paper is to apply this technique to investigate the three-dimensional instantaneous structures of an SWTBLI at Mach 3. The unsteady shock motion and the time evolution of the interaction are investigated in the streamwise wall-normal plane, and the three-dimensionality of the SWTBLI is visualized in the streamwise-spanwise planes at different heights.

2 Experimental apparatus and methods

2.1 Flow facility

The experiments reported in the present paper were performed in a supersonic wind tunnel in the Aerodynamics Laboratory of the National University of Defense Technology (see Fig. 1). The tunnel operates in a vacuum-indraft mode. The Mach number ranging from 2 to 3.8 can be set by using different nozzles. The test section is 250 mm long, 120 mm high, and 100 mm wide; each wall has a glass window along the entire test section length, providing ample optical access from four sides. In the present study, the tunnel was operated at Mach 3.0 with a stagnation pressure of 0.1 MPa and a stagnation temperature of 300 K. The test time was about 10 s at these conditions. The test boundary layer developed in a nominally zero pressure gradient along the wall of the wind tunnel, with transition occurring naturally upstream, in the nozzle section. The experimental conditions and the incoming turbulent boundary layer parameters are summarized in Table 1. The boundary layer parameters were acquired from high resolution particle image velocimetry (PIV) measurements at the same experimental conditions by He et al. [26].

A wedge with a flow deflection angle of 14° was used to generate the incident shock wave. It was placed in the freestream and spanned approximately the entire test section width. A schematic representation of the experimental arrangement and the photo of the model in the test section are shown in Fig. 2a, b, respectively. A Cartesian coordinate system is adopted with x, y, and z axes being along the streamwise, wall-normal, and spanwise directions, respectively. The origin is located at the extrapolated point of the incident shock wave impact on the wall. In the present study, instantaneous structures of the SWTBLI were visualized in the streamwise wall-normal plane (xy-plane) along the centerline of the test

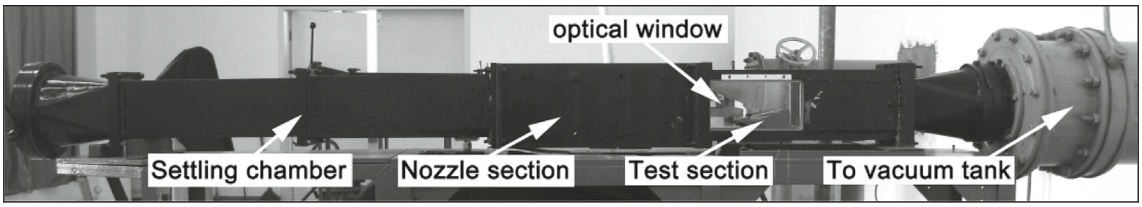

Fig. 1 Photo of the supersonic wind tunnel

Table 1 Experimental conditions and incoming turbulent boundary layer properties

Parameter	Description	Value
Ma	Free-stream Mach number	3.0
P_0	Stagnation pressure	0.1 Mpa
T_0	Stagnation temperature	300 K
U_∞	Free-stream velocity	620 m/s
Re	Reynolds number per meter	7.49×10^6 m^{-1}
δ	Boundary layer thickness	10.2 mm
δ^*	Displacement thickness	3.66 mm
θ	Momentum thickness	0.68 mm
δ^*/δ	δ^* to δ ratio	0.36
θ/δ	θ to δ ratio	0.067
$H = \delta^*/\theta$	Shape factor	5.38
Re_θ	Reynolds number based on θ	5,100
Re_δ	Reynolds number based on δ	76,500
u_τ	Friction (or shear) velocity	29.9 m/s
C_f	Skin friction coefficient	1.70×10^{-3}

section, and the streamwise-spanwise planes (xz-planes) at different heights above the wall.

2.2 NPLS technique

To visualize the three-dimensional instantaneous structure of SWTBLI, the NPLS technique was applied, which has recently been developed in our laboratory. The advantage of the NPLS technique is that it utilizes nanoparticles as tracers, which provides better flow-following ability of seed particles in supersonic and hypersonic flows. Besides, the scattering cross-section of nanoparticles is larger than that for molecular tracers, which results in stronger scattering signal so that an unintensified charge couple device (CCD) camera may be used for flow visualization instead of expensive intensified CCD (ICCD) cameras. Previous experimental results demonstrated that the NPLS technique is a useful tool for visualizing the structure of various supersonic flows [23–25].

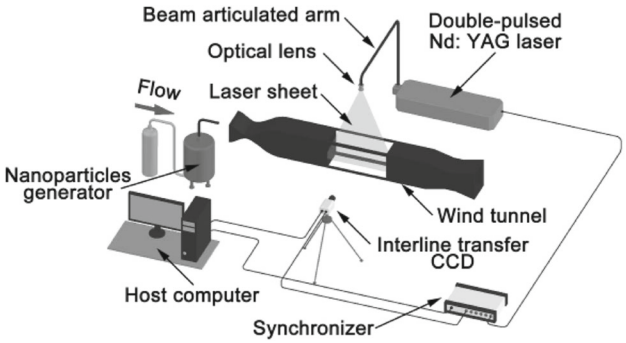

Fig. 3 Schematic of the NPLS system

In the present experimental studies, titanium dioxide (TiO_2) particles with a manufacturer-specified nominal particle diameter of 18 nm and a bulk density of approximately 300 kg/m^3 were adopted as seed particles (the actual particle size would be larger than the manufacturer-specified size due to the agglomeration effect). The seed particles were illuminated by a double-pulsed Nd:YAG Laser, with 500 mJ pulsed energy and a 6 ns pulse duration at wavelength 532 nm. The laser beam was delivered by an articulated arm and transformed into a laser sheet with a minimum thickness of about 0.5 mm using cylindrical and spherical lenses. The scattering by nanoparticles is in the Rayleigh regime since the nanoparticles have a characteristic size of the order of (or less than) the wavelength of incident light. A 12-bit interline transfer CCD camera, with a resolution of 2,048 × 2,048 pixels, is used as the imaging system which can capture two sequential images in a short time interval (sub-microsecond range). The double-pulsed Nd:YAG laser and CCD camera were connected to a host computer via a synchronizer, which controls the timing of laser illumination and image acquisition. The particles were seeded upstream of the stagnation chamber of the tunnel using a nanoparticle generator driven by compressed gas. A schematic depicting the NPLS system is shown in Fig. 3.

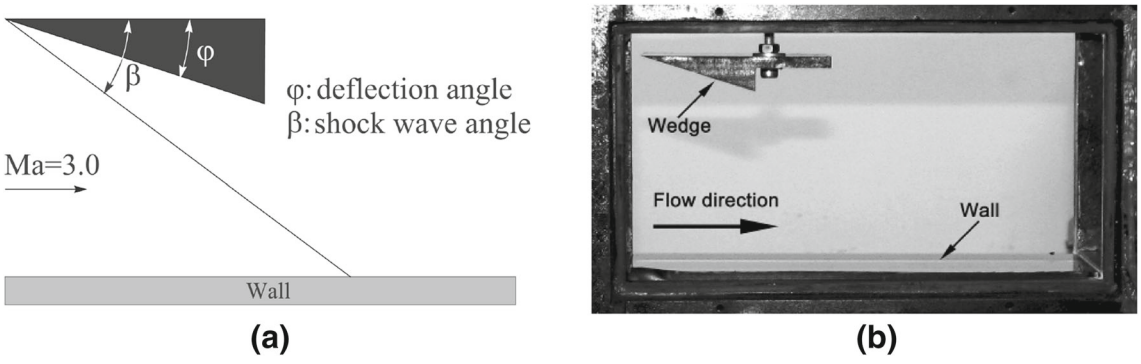

Fig. 2 Experimental arrangement. **a** Schematic of the experimental arrangement. **b** Photo of the model in the test section

3 Results and discussion

3.1 Streamwise structures of the SWTBLI

Figure 4 provides an overview of the basic features of the SWTBLI in the *xy*-plane. For comparison, a typical visualization result is shown Fig. 5. The field of view is $8\delta \times 3\delta$ (streamwise length × wall-normal length) with a digital resolution of approximately, 43.5 μm/pixel. The flow direction is from left to right. To interpret the NPLS image, the relation between the gray value of the NPLS image and the gas density must be considered. Due to the good flow-following ability of nanoparticles used in the NPLS technique, the local concentration of nanoparticles should be proportional to the local gas density, if the concentration distribution of particles at the flow inlet cross-section is uniform. Since the gray value of the NPLS image is determined by the intensity of scattered light, which is directly proportional to the local concentration of nanoparticles, the local gas density will be low in the low gray value (dark) region of the NPLS image, and vice versa. Therefore, a shock wave can be identified as the interface across which the gray value suddenly rises, due to the gas density increase across the shock.

In Fig. 5, the incident shock wave is clearly discernible in the upstream region, and the shock-wave angle measured from the image is 31.2°, which agrees well with the value calculated from the oblique shock relations with the deflection angle of 14°. The incident shock is strong enough to induce the separation of the incoming turbulent boundary layer. The separation point (labeled as S) can be roughly designated to be at the location where the boundary layer is lifted away from the wall, as seen on the NPLS image. Compression waves are induced by the separation bubble. They coalesce to form the reflected shock wave, which thus originates upstream from the extrapolated wall impact point of the incident shock. The intersection of the incident shock with the reflected shock causes the formation of a slip line, which is observed to bend towards the wall through the expansion region and then turn parallel to the wall after the reattachment shock. Unlike within the shock waves, the density gradient in the expansion region is small, so that the location of expansion waves cannot be identified accurately in the NPLS image. The separation bubble ends at the reattachment point R, which can be estimated to be at the location where the boundary layer eventually reattaches to the wall. The newly developing boundary layer is observed downstream from the reattachment point.

The spatial structure of the SWTBLI observed in Fig. 5 is consistent with that shown in Fig. 4, schematically. Compared with schlieren images, which represent a spanwise average of density gradients, the NPLS technique can visualize instantaneous three-dimensional structures of supersonic flows. The large-scale structures within the incoming boundary layer are clearly discernible. However, such structures become irregular further downstream, as a result of the interaction process.

The four NPLS images shown in Fig. 6 display the instantaneous global structure of the SWTBLI at different times; each image is uncorrelated in time because the time that elapses between consequent recordings (a maximum framing rate of 15 Hz) is significantly greater than any characteristic flow time scale. The comparison of the instantaneous structures reveals unsteady features of the SWTBLI. In the freestream region, the flow remains steady and no appreciable motion of the incident shock wave can be detected. On the contrary, the incoming turbulent boundary layer exhibits strong unsteadiness, and the intermittent nature of the boundary layer edge can also be observed. The separation bubble also appears to be highly unsteady; the separation and reattachment points move upstream and downstream. The reflected shock appears to move upstream when the separation point moves in the same direction, and vice versa. Besides, the reflected shock moves away from the wall when the thickness of the incoming boundary layer increases. This suggests that the large-scale motion of the reflected shock wave is associated with the motion of the separation bubble as well as with the thickness of the incoming boundary layer.

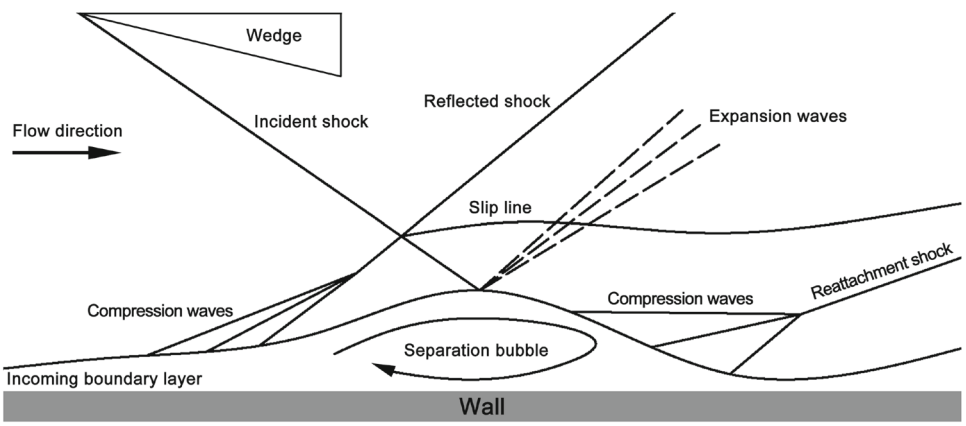

Fig. 4 A sketch of the SWTBLI in the *xy*-plane

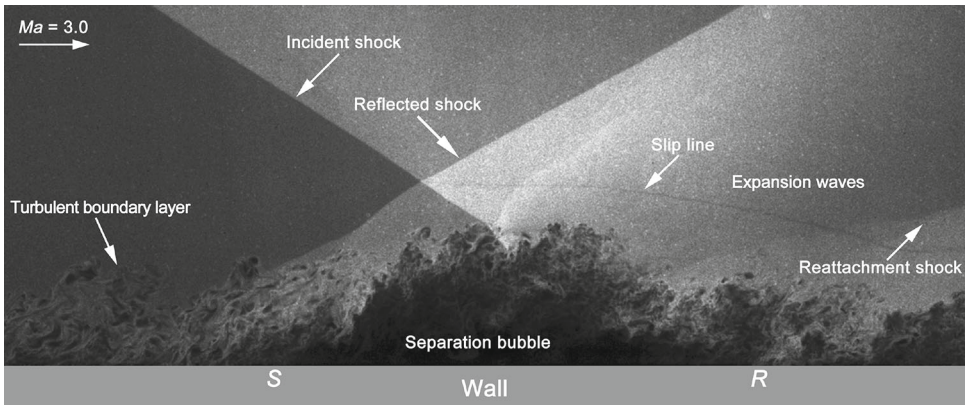

Fig. 5 A NPLS image of the instantaneous structure of the SWTBLI in the *xy*-plane (the flow is from *left* to *right*)

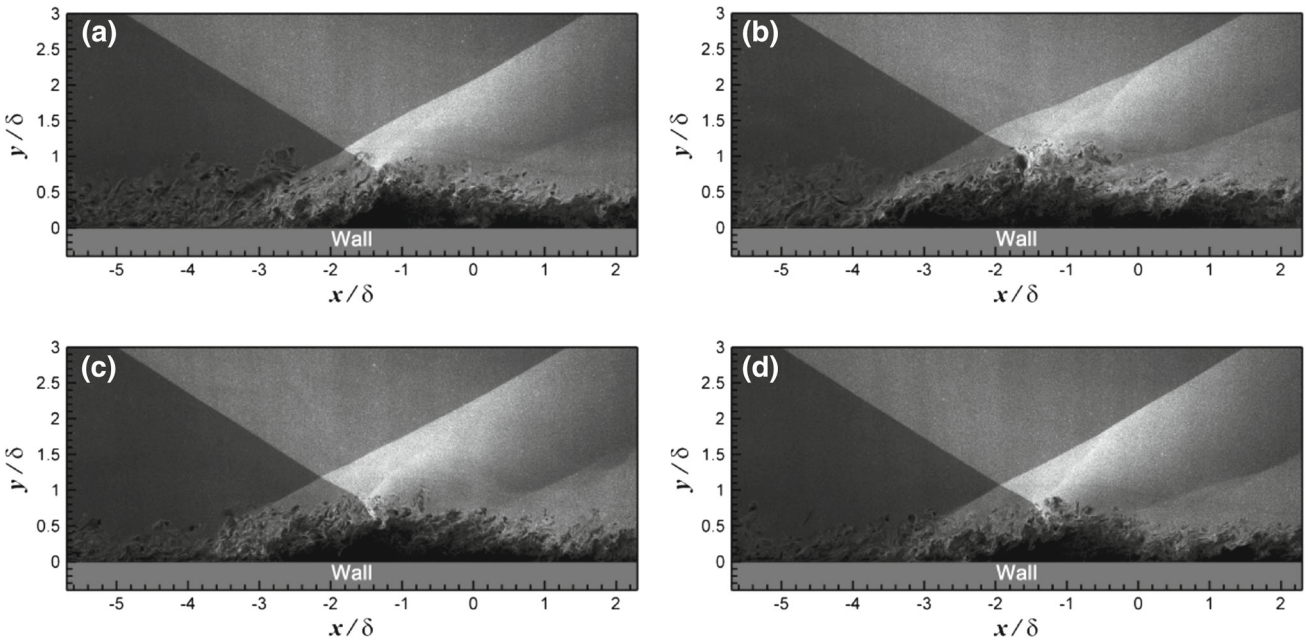

Fig. 6 Comparison of the instantaneous structure of the SWTBLI at different times (the flow is from *left* to *right*)

The separation point is roughly estimated to be at $x/\delta = -2.6$ in Fig. 6a but moves upstream to $x/\delta = -3.6$ in Fig. 6b, while the thickness of the incoming boundary layer is nearly the same. However, the instantaneous structures of the boundary layer are quite different from each other. Comparing Fig. 6a, c, it can be seen that the location of the separation point does not change significantly when the boundary layer thickness obviously changes. Thus, the interaction unsteadiness may not be associated with the thickness of the incoming boundary layer. Instead, a relationship between the instantaneous structures within the incoming boundary layer and the unsteady behavior of the interaction may exist; however, the underlying physical mechanisms are still not well-understood. Some recent experimental evidence also suggests that the separation shock unsteadiness may be associated with the velocity fluctuations within the upstream boundary layer, which should be related to the instantaneous structures [27–29].

Using the double-pulsed Nd:YAG laser and the interline transfer charge-couple device (CCD) camera, a series of image pairs (5 image pairs per second) can be obtained during each experiment. The time interval between two images of each pair is very short (microsecond range). These image pairs will help to improve our understanding of the time evolution of the SWTBLI, if the structures would remain recognizable during the time interval.

An example is shown in Fig. 7. The time delay between the two images is 10 μs, and the flow is from left to right. The field of view is the same as that displayed in Fig. 5. Three typical large-scale structures are selected and indicated by the circles. After 10 μs (lower image), these structures are still recognizable, despite some changes in their shapes. The dis-

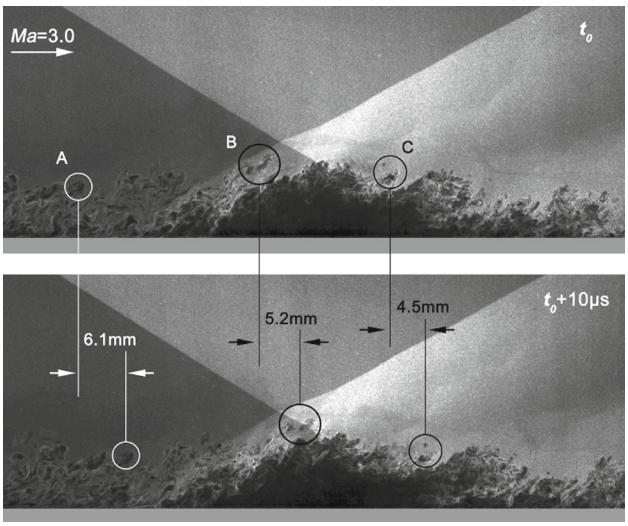

Fig. 7 Successive NPLS images of the SWTBLI; the flow is from *left* to *right*, and the time delay is 10 μs

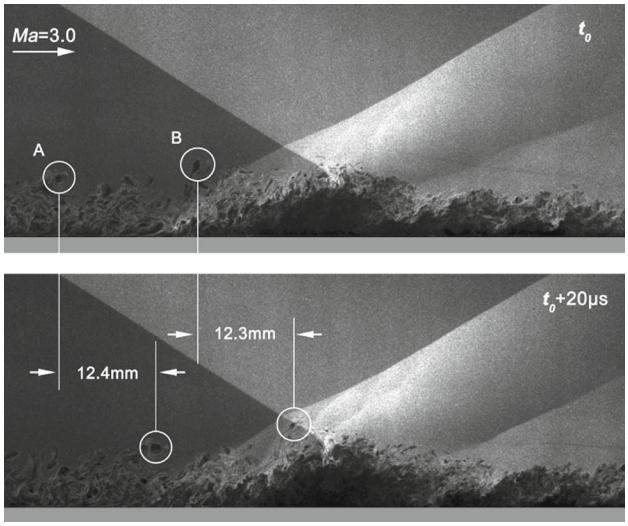

Fig. 8 Successive NPLS images of the SWTBLI; the flow is from *left* to *right* and the time delay is 20 μs

placement of the large-scale structure in region A (structure A) during that time is roughly estimated from the two images to be 6.1 mm. The corresponding mean streamwise velocity is nearly equal to the freestream velocity. In the interaction region, the structure B moves away from the wall, and the streamwise displacement is smaller (5.2 mm) due to the flow deceleration after the reflected shock. As can be observed in the lower image, the structure B is just passing through the incident shock at this moment. The structure C is observed to move toward the wall; the streamwise displacement is only 4.2 mm as the flow is decelerated again after the incident shock. From direct comparison of the two images, it is found that, during the 10 μs interval, the flow structures have propagated downstream with some changes in the geometry of smaller-scale structures. However, the large-scale structures in the interaction zone become more irregular than those in the incoming boundary layer. This may be due to the effect of the incident and reflected shock waves, which induce more complex interactions between turbulent structures. Therefore, there are relatively large changes in the shape of coherent structures in the interaction zone over the time interval. It is interesting that the structure B is still recognizable, even though it interacts with the incident shock directly. This means that the evolution of the large-scale structures induced by the shock waves could be a relatively slow process.

As the time delay is increased to 20 μs, the large-scale structures in the incoming boundary layer are still recognizable, as shown in Fig. 8. The structure A is convected downstream at the speed equal to the freestream velocity, and its size and distance from the wall are increased. It is also interesting to note that this structure exhibits a tendency to rotate clockwise, which might correspond to a hairpin head in the outer region of the turbulent boundary layer. The structure B

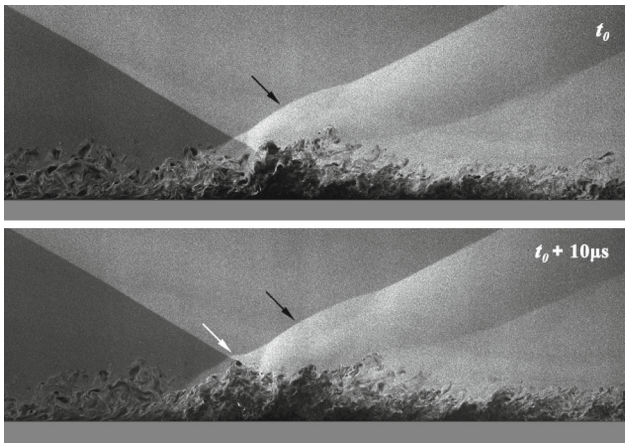

Fig. 9 Successive NPLS images of the interaction between the large-scale structures and the reflected shock; the flow is from *left* to *right*, and time delay is 10 μs

also shows the same tendency but its size is decreased. However, the structures in the interaction zone cannot be easily identified due to significant changes in their shape and size.

It should be noted that, despite the remarkable changes of small-scale structures, the shape and location of both the separation bubble and the reflected shock remain the same during the 20 μs interval. According to Fig. 6, the separation bubble and the reflected shock do exhibit strong unsteadiness. This means that the time scale of the separation bubble motion is much larger than 20 μs, which is nearly equal to the characteristic time scale of the incoming boundary layer (δ/U_∞). As mentioned above, several previous studies reported that the time scale of the large-scale low-frequency motion is of the order of $10\ \delta/U_\infty - 100\,\delta/U_\infty$ [1,21,22]. However, in the present experiment, we cannot determine the time scale

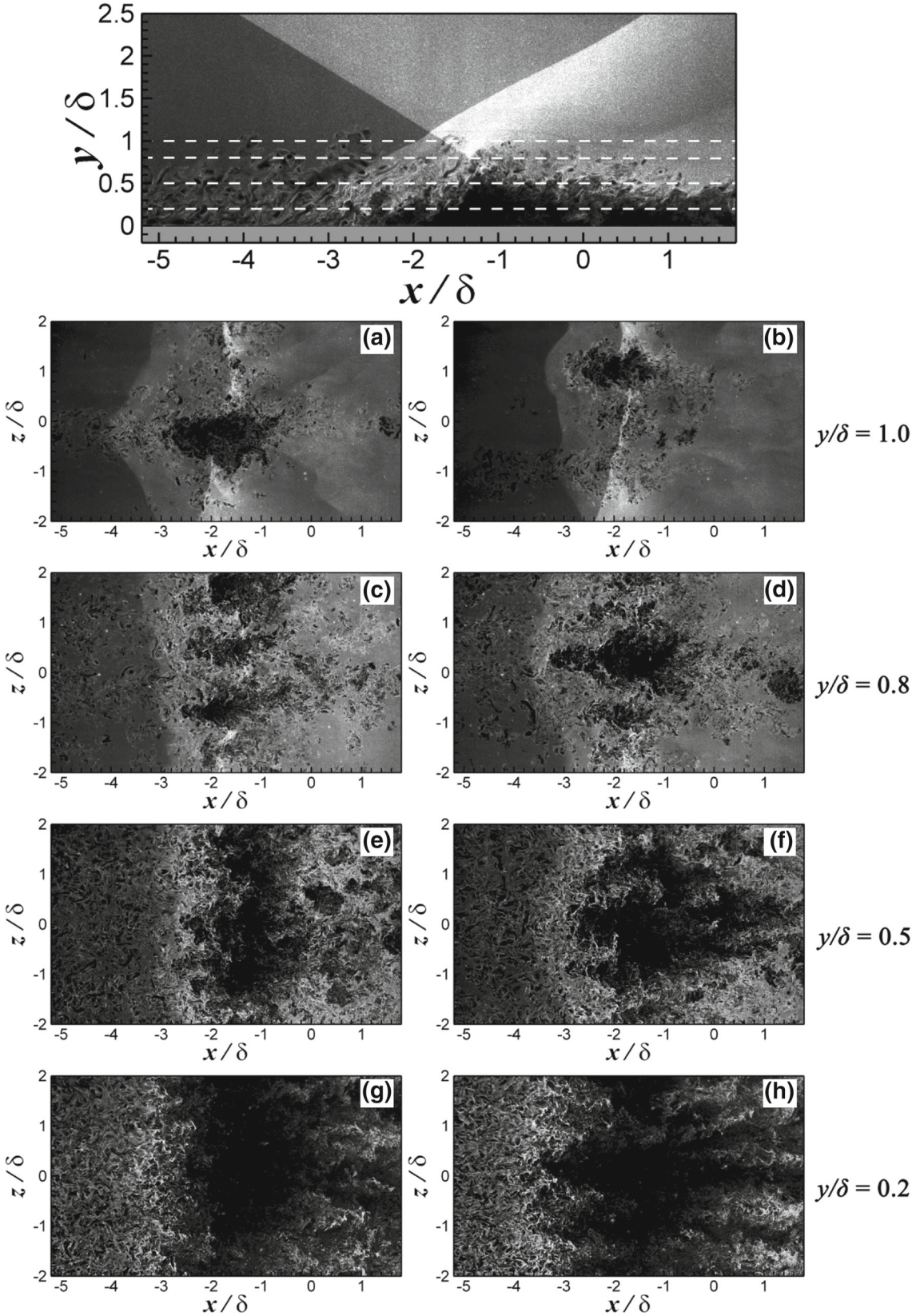

Fig. 10 NPLS images of the SWTBLI in the *xz*-plane at different heights; the flow is from *left* to *right*. Each image was not obtained simultaneously

of the separation bubble motion using only two successive images.

As shown in the upper image of Fig. 9, a curved section of the reflected shock can be observed, as pointed out by the black arrow. After 10 μs delay, this structure has moved downstream. The curved section resembles a bow shock generated by the large-scale structures very close to it in the downstream direction, which would explain why the curved section became flatter when the large structures moved away from it in the lower image. It is also interesting to observe that, when a large structure in the incoming boundary layer enters the interaction zone, a new curved section of the reflected shock is generated, as indicated by the white arrow in the lower image. This suggests that the flow behind the reflected shock and even the incident shock is still supersonic relative to the large-scale structures in the separated boundary layer, and these curved sections of the reflected shock are eddy shocklets. However, the reflected shock remains a straight line and does not move upstream or downstream in the freestream, when affected by the large-scale structures in the near wall region.

3.2 Spanwise structures of the SWTBLI

A series of NPLS images obtained in the xz-plane at four different heights is shown in Fig. 10. The field of view is $7\delta \times 4\delta$ (streamwise length × spanwise length) with a digital resolution of approximately 43.5 μm/pixel, and the flow is from left to right. In each xz-plane, two independent NPLS images are selected to exhibit the unsteady nature of the interaction. For the purpose of comparison, a streamwise image is also placed at the top of Fig. 10, with the white dashed lines indicating each y/δ location in the xy-plane. It is to be noted that all images presented here were not obtained simultaneously.

As seen in Fig. 10g, the separated region is nearly rectangular in shape at $y/\delta = 0.2$, ranging from approximately $x/\delta = -3$ to 0. However, it exhibits some three-dimensionality in Fig. 10h. Along the z direction, the location of the separation point is varied from $x/\delta = -3.8$ to -2. This may be caused by the high- and low-speed fluids in the upstream boundary layer, though such structures cannot be identified in the NPLS images as reported in Ref. [26]. Elongated streaks in the streamwise direction are clearly visible downstream from the separated region. The comparison with Fig. 10g suggests that the occurrence of such elongated streaks is probably due to the three-dimensional nature of the separation bubble. In addition, both the reflected shock and the incident shock are not observed at this y/δ location.

At $y/\delta = 0.5$, the length of the separated region in the streamwise direction decreases. There is a rather significant change in the shape of the separation bubble. It exhibits a rectangular shape in Fig. 10e but changes to a diamond shape in Fig. 10f. According to the method mentioned above, a compression wave can be identified in the NPLS images at this location. It is approximately a straight line in Fig. 10g but exhibits an arch shape in Fig. 10f, which is consistent with the change of the separation bubble.

The top part of the separation bubble can be observed at $y/\delta = 0.8$; its shape and location vary randomly. For example, in Fig. 10c the separation bubble is divided into three sections of nearly the same size, aligned in the spanwise direction. But in Fig. 10d it consists of a bigger section accompanied by a small one. Besides, the distance between the compression wave (or it may be the reflected shock at this location) and the separation bubble is increased from Fig. 10c to d.

At the location of $y/\delta = 1.0$, a long streak along the streamwise direction can be seen in Fig. 10a and b, which indicates that the local thickness of the incoming boundary layer is larger than the mean thickness ($\delta = 10.2$ mm). Such structures may correspond to the organized vortices in the outer region of the turbulent boundary layer, as mentioned by Adrian et al. [30]. A separation bubble can be found just downstream from the long streak in Fig. 10a. On the contrary, the separation bubble is not visible downstream from the long streak in Fig. 10b. At the same time, no streak structures can be observed upstream from the separation bubble in Fig. 10b. This would imply that there is no significant correlation between the local boundary layer thickness just upstream of the interaction zone and the separation bubble location, as reported by Chan [17] and Beresh et al. [18]. Besides, the incident shock can be identified downstream from the reflected shock but it is not visible in the separated region at this location. Theoretically, the reflected shock should be a straight line in the xz-plane, but in fact it is curved along the z direction. Furthermore, the reflected shock does not move appreciably at different times, as compared to what is observed in the streamwise plane.

The randomness of the separation bubble, both in position and shape, increases away from the wall, while its size decreases. Although the existence of two counter-rotating tornado-like vortices within the interaction region was reported by Dussauge et al. [22], such structures cannot be identified in the NPLS images. The instantaneous structures in the spanwise planes suggest strong three-dimensionality of the SWTBLI. Therefore, the structures in the interaction zone will be influenced not only by the fluctuations in the upstream boundary layer but also by the surrounding fluid due to the three-dimensional nature. This could increase the complexity of the interaction unsteadiness.

4 Conclusions

Flow visualization experiments were performed to investigate the three-dimensional instantaneous structures of SWT-

BLI at Mach 3. The flow structures in both the streamwise wall-normal (*xy*-) and streamwise-spanwise (*xz*-) planes were obtained using the NPLS technique.

In the *xy*-plane, large-scale structures can be identified within the incoming turbulent boundary layer; its thickness changes in time, exhibiting the intermittent nature of the turbulent boundary layer. The separation bubble moves upstream and downstream at different times, and the motion of the reflected shock is associated with the separation bubble; these represent the unsteady features of the SWTBLI. The unsteady motion of the separation bubble is not associated with the change of the upstream boundary layer thickness.

The time evolution of the structures was investigated using two successive NPLS images with a very short time interval. After a certain time, the large-scale structures in the interaction zone become more irregular than those in the incoming boundary layer, which may be due to the effect of shock waves. However, the time scale of the separation bubble motion is much larger than the characteristic time scale of the incoming boundary layer. Curved sections of the reflected shock can be observed due to the effect of the large-scale structures in the near wall region, which resemble eddy shocklets.

The instantaneous structures in different *xz*-planes suggest strong three-dimensionality of the SWTBLI. The size of the separated region decreases away from the wall. The shape of the reflected shock in the *xz*-plane is closely associated with the shape of the separation bubble. Large-scale motions within the incoming turbulent boundary layer were observed, which do not, however, affect the unsteady features of the interaction. The underlying physical mechanism of the interaction unsteadiness would become even more complex, when taking into account the three-dimensionality of the flow.

Acknowledgments This research was supported by the National Basic Research Program of China (No. 2009CB724100) and the National Natural Science Foundation of China (Grant No. 11172326).

References

1. Dolling, D.S.: Fifty years of shock-wave boundary layer interaction research: What Next? AIAA J. **39**, 1517–1531 (2001)
2. Smits, A.J., Dussauge, J.P.: Turbulent shear layers in supersonic flow, 2nd edn. Springer, New York (2006)
3. Dupont, P., Haddad, C., Debiève, J.-F.: Space and time organization in a shock-induced separated boundary layer. J. Fluid Mech. **559**, 255–277 (2006)
4. Chapman, D.R., Kuhen, D.M., Larson, H.K.: Investigation of separated flows in supersonic and subsonic streams with emphasis on the effect of transition. NACA TN-3869 (1957)
5. Verma, S.B., Koppenwallner, G.: Detection of shock motion using laser schlieren system in a hypersonic SWBLI flowfield. AIAA Paper 2001–1756 (2001)
6. Verma, S.B.: Detection of fluctuating density gradient flow field in shock wave boundary layer interactions using laser Schlieren system. Exp. Fluids **32**, 527–531 (2002)
7. Debiéve, J., Ardissone, J., Dussauge, J.: Shock motion and state of turbulence in a perturbed supersonic flow around a sphere. J Turb **4**, 1–15 (2003)
8. Kastengren, A.L., Dutton, J.C., Elliott, G.S.: A method for measuring recompression shock unsteadiness applied to two supersonic wakes. Exp. Fluids **39**, 140–151 (2005)
9. Souverein, L.J., Debieve, J.F.: Effect of air jet vortex generators on a shock wave boundary layer interaction. Exp. Fluids **49**, 1053–1064 (2010)
10. Humble, R.A., Scarano, F., van Oudheusden, B.W.: Particle image velocimetry measurements of a shock wave/turbulent boundary layer interaction. Exp. Fluids **43**, 173–183 (2007)
11. Clemens, N., Mungal, M.: A planar Mie scattering technique for visualizing supersonic mixing flows. Exp. Fluids **11**, 175–185 (1991)
12. Clemens, N., Mungal, M.: Large-scale structure and entrainment in the supersonic mixing layer. J. Fluid Mech. **284**, 171–216 (1995)
13. Smith, K.M., Dutton, J.C.: Investigation of large-scale structures in supersonic planar base flows. AIAA J. **34**, 1146–1152 (1996)
14. Bourdon, C.J., Dutton, J.C.: Planar visualizations of large-scale turbulent structures in axisymmetric supersonic separated flows. Phys. Fluids **11**, 201–213 (1999)
15. Kastengren, A.L., Dutton, J.C.: Wake topology in a three-dimensional supersonic base flow. AIAA paper 2004–2340 (2004)
16. Smith, M.W., Smits, A.J.: Visualization of the structure of supersonic turbulent boundary layers. Exp. Fluids **18**, 288–302 (1995)
17. Chan, S.C.: Planar laser scattering imaging of shock wave turbulent boundary layer interactions. M.S. Thesis, Dept. of Aerospace Engineering and Engineering Mechanics, The University of Texas at Austin, USA (1996)
18. Beresh, S.J., Clemens, N.T., Dolling, D.S., Comninos, M.: Investigation of the causes of large-scale unsteadiness of shock-induccd separated flow using planar laser imaging. AIAA Paper 97–0064, (1997)
19. Ganapathisubramani, B., Clemens, N.T., Dolling, D.S.: Planar imaging measurements to study the effect of spanwise structure of upstream turbulent boundary layer on shock induced separation. AIAA Paper 2006–324 (2006)
20. Wu, P., Miles, R.B.: MHz rate visualization of separation shock wave structure. AIAA Paper 2000–0647 (2000)
21. Wu, M., Martin, M.P.: Analysis of shock motion in shockwave and turbulent boundary layer interaction using direct numerical simulation data. J. Fluid Mech. **594**, 71–83 (2008)
22. Dussauge, J.P., Dupont, P., Debiève, J.F.: Unsteadiness in shock wave boundary layer interactions with separation. Aero. Sci. Technol. **10**, 85–91 (2006)
23. Zhao, Y.X., Yi, S.H., He, L., Cheng, Z.Y., Tian, L.F.: The experimental study of interaction between shock wave and turbulence. Chinese Sci. Bull. **52**, 1297–1301 (2007)
24. Zhao, Y.X., Yi, S.H., Tian, L.F., He, L., Cheng, Z.Y.: The fractal measurement of experimental images of supersonic turbulent mixing layer. Sci. China Ser. G: Phys. Mech. Astron. **51**, 1134–1143 (2008)
25. He, L., Yi, S.H., Zhao, Y.X., Tian, L.F., Chen, Z.: Visualization of coherent structures in a supersonic flat-plate boundary layer. Chinese Sci. Bull. **56**, 489–494 (2011)
26. He, L., Yi, S.H., Zhao, Y.X., Tian, L.F., Chen, Z.: Experimental study of a supersonic turbulent boundary layer using PIV. Sci. China, Ser. G: Phys. Mech. Astron. **54**(9), 1702–1709 (2011)
27. Beresh, S.J., Clemens, N.T., Dolling, D.S.: Relationship between upstream turbulent boundary layer velocity fluctuations and separation shock unsteadiness. AIAA J. **40**(12), 2412–2422 (2002)

28. Beresh, S.J., Clemens, N.T., Dolling, D.S.: The relationship between upstream turbulent boundary layer velocity fluctuations and separation shock unsteadiness. AIAA Paper 99–0295 (1999)
29. Ganapathisubramani, B., Clemens, N.T., Dolling, D.S.: Effects of upstream boundary layer on the unsteadiness of shock-induced separation. J. Fluid Mech. **585**, 369–394 (2007)
30. Adrian, R.J., Meinhart, C.D., Tomkins, C.D.: Vortex organization in the outer region of the turbulent boundary layer. J. Fluid Mech. **422**, 1–54 (2000)